Deep Resources Engineering 3 (2026) 100235

Contents lists available at ScienceDirect

Deep Resources Engineering

journal homepage: www.keaipublishing.com/en/journals/deepre/

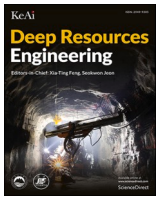

Full length article

Mechanism of transient phase transition in liquid oxygen with different absorbent media

Yanbing Wang [a,*], Xue Li [a], Dairui Fu [a], Kangcheng Li [a], Dongchen Wang [a], Haitao Le [b], Linsheng Zhao [b], Chuanhao Lv [c], Yuanyuan Liu [c], Bo Xu [d], Zungang Liu [d], Xiao Wang [e]

[a] School of Mechanics and Civil Engineering, China University of Mining and Technology, Beijing 100083, China
[b] Guangxi Guofang Construction Engineering Co., Ltd., Nanning, Guangxi 530033, China
[c] Baorong Shengwei (Shenyang) Technology Co., Ltd., Shenyang, Liaoning 110000, China
[d] Wenshang Yiqiao Coal Mine Co., Ltd., Jining, Shandong 272500, China
[e] Beijing Zhongda Blasting Engineering Co., Ltd., Beijing 102200, China

ARTICLE INFO

Keywords:
Absorbent media
Liquid oxygen transient phase transition
High-speed photography
Vaporization-expansion
Fiber structure

ABSTRACT

This study captures transient phase change reaction images of dual liquid oxygen charges with different absorbent media in the same frame using a high-speed camera. Based on grayscale image temporal features, the transient phase change reaction process of liquid oxygen charges with different media is divided into three stages: initial combustion, gasification expansion, and turbulent dissipation. By inverting the relative velocity and temperature fields from grayscale images, the differences in phase change processes among various absorbent media are analyzed, exploring the characteristic differences of absorbent media with different fiber structures across reaction stages. The study reveals that tissue paper, as a porous short-fiber material, releases energy steadily, while cotton, with its dense long-fiber structure, exhibits concentrated energy release with a longer time delay due to lower permeability. Under identical initiation times, tissue paper shows a more uniform reaction velocity distribution compared to cotton, which produces transient high-speed points. The phase change uniformity of tissue paper is significantly higher than that of cotton, indicating that the short-fiber structure of tissue paper has a superior liquid oxygen adsorption capacity compared to cotton. Although cotton generates higher local pressure, the uneven adsorption of liquid oxygen leads to a significantly lower energy utilization efficiency and non-uniform energy release. As a potential indicator reflecting rock-breaking performance, this difference in energy utilization demonstrates that the liquid oxygen charge with cotton as the absorbent media exhibits inferior potential rock-breaking performance compared to that using toilet paper as the absorbent media.

1. Introduction

With the acceleration of urbanization in China, the demand for urban underground infrastructure construction, underground space development, and geological disaster prevention is increasing. Rock breaking and excavation remain core challenges in engineering construction [1, 2]. Traditional explosive blasting, which releases energy instantaneously and transmits high-energy shock loads through detonation waves, is widely used in large-scale rock excavation, mining, and demolition. However, its inherent high risks, vibrations, and strict regulations no longer meet current stringent environmental and safety requirements. Therefore, developing more environmentally friendly and safer controllable energy release technologies has become an urgent research direction.

The rise of gas expansion rock-breaking technology has achieved controllability in energy output [3–6]. High-pressure gas expansion rock-breaking technology primarily uses liquid carbon dioxide, liquid nitrogen, or liquid oxygen as raw materials, triggering phase changes through initiation devices to release high-energy shock waves [7]. Liquid carbon dioxide blasting technology has been studied by Qin, Wang, and Cheng et al. [8–10] through laboratory experiments and numerical simulations to explore influencing factors in rock excavation. Liquid nitrogen blasting technology has been investigated by Lin and Wang et al. [11–13] to analyze pressure changes during the phase change process for rock-breaking mechanisms. Liquid oxygen expansion rock-breaking technology, as an emerging green gas-based

* Corresponding author.
E-mail address: wangyanbing@cumtb.edu.cn (Y. Wang).

https://doi.org/10.1016/j.deepre.2025.100235
Received 4 October 2025; Received in revised form 4 December 2025; Accepted 18 December 2025
Available online 25 December 2025

rock-breaking method, has gained attention in recent years [14–16]. Unlike traditional explosive blasting, liquid oxygen expansion technology utilizes the phase change characteristics of liquid oxygen to break rock through the release of expanding gases, significantly reducing blasting vibrations and harmful gas emissions. Additionally, the high energy density and instantaneous expansion properties of liquid oxygen provide unique advantages in precisely controlling blasting energy and effects. However, challenges remain in practical applications, particularly in the effective control of energy and the release process of expanding gases during liquid oxygen blasting, especially the influence mechanisms of different absorbent media on the liquid oxygen expansion process and rock-breaking effects, which have not been fully elucidated.

The absorbent media, a critical component of liquid oxygen charges, regulates the phase change rate and gas expansion characteristics while influencing the distribution and transmission of blasting energy through its adsorption capacity, thereby affecting pressure release characteristics and rock-breaking outcomes [17]. Although common absorbent materials are inorganic chemicals, organic absorbent materials like tissue paper and cotton, with their unique fiber structures and adsorption properties, offer new research directions for liquid oxygen expansion rock-breaking. The rapid water absorption of tissue paper and the efficient fiber structure of cotton enable them to regulate expansion rates and blasting energy release during liquid oxygen phase changes. These materials are cost-effective, environmentally friendly, and capable of altering gas expansion characteristics through their physical properties, thus enhancing rock-breaking effects. However, research on the impact of different absorbent media on the liquid oxygen blasting process, particularly in terms of microscopic dynamics and energy release mechanisms, remains limited, necessitating systematic experimental and theoretical analysis to address this gap.

The present work establishes a comprehensive analysis system based on high-speed schlieren image sequences of liquid oxygen blasting with different absorbent media, covering image enhancement, edge detection, thermal inversion, and propagation modeling. It quantifies the evolution of phase change front morphology, flame-shock wave coupling propagation behavior, and heat release patterns under different absorbent media. The study analyzes the regulatory effects of tissue paper and cotton on the liquid oxygen response process, revealing the physical mechanisms of porous media in coupled thermal-flow reactions and providing a theoretical basis for energy control in liquid oxygen charges.

2. Research method

2.1. Experimental design

The experimental system comprises a charge system, a blasting monitoring system, a liquid filling system, an ignition system, and a blast protection system. As shown in Fig. 1, the charge structure with a length of 50 mm and a diameter of 150 mm, consists of an ignition head, detonation wire, absorbent media, liquid filling tube, gas exhaust tube, inner liquid storage tube, and outer liquid storage tube. The ignition head is connected to the detonation wire and a remote control system, synchronized with a high-speed camera to capture liquid oxygen blasting while initiating electric ignition. The absorbent media contains the ignition head, detonation wire, liquid filling tube, and exhaust tube, placed within the inner liquid storage tube and wrapped with sealing tape. The inner liquid storage tube, made of plastic film, is fixed and sealed before being installed into the outer liquid storage tube made of PVC. After the inner liquid storage tube is fixed and sealed, the outer liquid storage tube is installed. The inner liquid storage tube is made of plastic film, and the outer one is made of PVC. The double-layer liquid storage tube structure ensures the tightness after liquid oxygen injection and is connected to an outer liquid filling system. The outer liquid filling system consists of a vertical Dewar tank and a liquid filling pipeline. The outer layer of the vertical Dewar tank adopts a vacuum insulation structure, and the liquid filling pipeline is wrapped with thermal insulation cotton and a water hose, achieving both thermal insulation and pipeline protection functions. The charge system and the liquid filling system are installed and transported separately, enabling on-site liquid oxygen blasting with immediate charging and detonation, thus further ensuring the safety of the experiment. During the experiment, two charges are fixed in the explosion-proof box with cable ties, and a suspended steel pipe is built in the center of the box. The two charges are tied to both sides of the suspended steel pipe respectively, placed on the same horizontal line, and their blasting processes with different medium structures are observed through synchronous detonation and in the same camera frame, eliminating systematic errors for direct comparison of phase transition processes.

In the experimental process, each subsystem in the test system is first connected, and the field of view of the blasting monitoring system is checked. After the connection and preparation of the test equipment are completed, liquid filling into the charges is started. The single oxygen charging time is set to 5 min, determined by the liquid oxygen charge being fully filled with liquid oxygen and a large amount of liquid oxygen spraying out from the exhaust pipe. Specifically, a saturated liquid

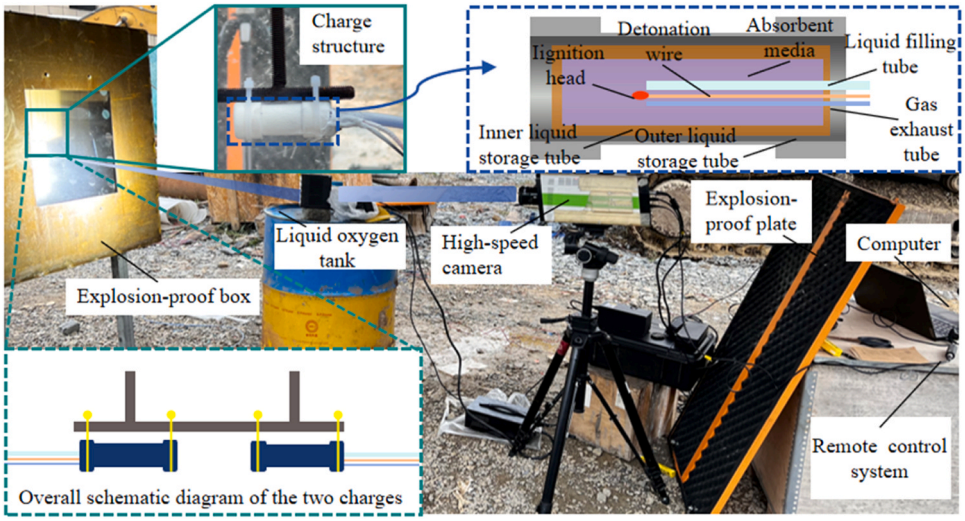

Fig. 1. Experimental system.

oxygen filling method is adopted to ensure sufficient and consistent liquid oxygen content inside the liquid oxygen charges of the same size. After liquid oxygen filling is completed, a synchronous controller and remote ignition control are used to trigger high-speed camera shooting and the electric detonation command of the charges, while recording the transient phase transition reaction processes of liquid oxygen charges with different absorbent media.

2.2. Test materials

To investigate the liquid oxygen adsorption capacity of low-cost absorbent media and the penetration and phase change processes of ultra-low-temperature liquids in porous media, tissue paper and cotton were selected, both being cellulose-based materials. Tissue paper has a loose, short-fiber porous structure, while cotton has a natural, dense, long-fiber structure. Tissue paper's porosity is significantly higher than that of cotton, resulting in a higher adsorption rate under identical filling times. As shown in Fig. 2, the experiment used approximately 1.5 g of each material to explore differences in the transient phase change reaction processes of liquid oxygen with these absorbent media and their distinct performances.

2.3. High-speed imaging system

The experiment utilized an X213 high-speed camera to capture the blasting process of liquid oxygen charges with different media, configured with an IP/SN of 192.168.8.7 to ensure stable data interaction. The equipment was set to internal synchronization mode with a pulse width of 1 μs to ensure signal synchronization accuracy. The acquisition window was set to manual mode with a frame rate of 100,000 fps and a resolution of 512 × 112, meeting the demands of high-speed image acquisition. The exposure time was set to 90 μs, adapted to the lighting conditions of the liquid oxygen phase change experiment. An internal trigger mode was used to simplify trigger control logic, ensuring the integrity of high-speed image data collection.

2.4. Data analysis method

2.4.1. Image processing techniques

In high-speed schlieren experiments, density disturbances, gas-phase expansion, and shock wave structures during the reaction process are reflected as bright and dark regions in images. Due to issues such as high-frequency noise, insufficient contrast, and edge blurring in schlieren images, image processing techniques were employed to process experimental images, mitigating the impact of noise and contrast issues on the accuracy of experimental data.

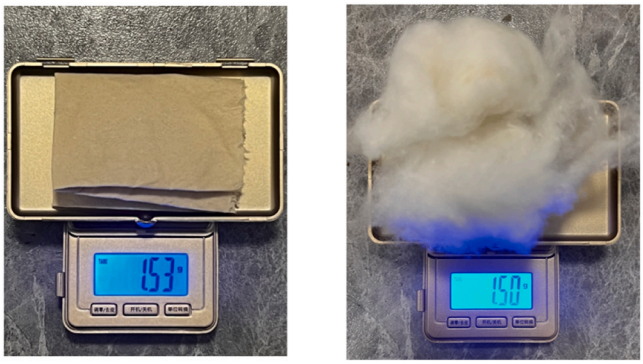

(a) (b)

Fig. 2. Different absorbent test materials: (a) tissue absorbent media; (b) cotton absorbent media.

2.4.2. Schlieren image sequence feature extraction algorithm

Schlieren image sequences record dynamic evolution information of the reaction process, particularly the position, morphology, and expansion trends of disturbance structures. To quantitatively characterize these features, this study employed edge detection and morphological processing to identify the contours of disturbance structures, extracting geometric parameters such as area, contour length, and maximum axis length. To obtain temporal characteristics of disturbance propagation, dense optical flow methods were used to calculate the frontal displacement of disturbance structures between adjacent frames, deriving the variation curve of disturbance propagation speed over time. By combining the area and propagation speed of disturbance regions, the volumetric expansion rate of these structures per unit time was estimated. By organizing these image features into time-series data, systematic input variables were provided for reaction kinetics modeling and parameter inversion.

2.4.3. Reaction kinetics parameter inversion model

The reaction process of liquid oxygen charges is influenced by environmental media, temperature fields, and reagent distribution, exhibiting significant nonlinear evolution characteristics. To derive microscopic kinetic parameters describing the reaction's essence from the disturbance structure data obtained from high-speed schlieren images, a reaction kinetics inversion model was established based on classical Arrhenius kinetics, incorporating disturbance geometric information and diffusion propagation behavior. The model assumes the reaction follows a single-step irreversible reaction, with the reaction rate per unit volume adhering to the Arrhenius formula:

$$R(t) = A \cdot \exp\left(-\frac{E_a}{RT(t)}\right) \cdot C(t)^n \tag{1}$$

where $R(t)$ is the reaction rate, mol/(m³·s); A is the Arrhenius factor, the frequency factor of the rate constant, 1/s; E_a is the activation energy, J/mol; R is the universal gas constant, J/ (mol·K); $T(t)$ is the temperature, K; $C(t)$ is the reactant concentration, mol/ m³ ; and n is the reaction order.

The volume change rate of the disturbance region is approximated as:

$$\frac{dV(t)}{dt} = \alpha \int_{V(t)} R(t) dV \tag{2}$$

where $V(t)$ is the volume of the reaction system at time t, m³ ; $\frac{dV(t)}{dt}$ is the volume change per unit time, m³ /s; α is a proportionality coefficient; and $\int_{V(t)} R(t) dV$ is the total reaction rate of the system at time t, mol/ s.

The volume growth rate of the disturbance structure can be obtained by multiplying the disturbance front speed $v(t)$ measured from schlieren images by the surface area $A_s(t)$:

$$\frac{A_s(t) \cdot v(t)}{V(t)} = \alpha \cdot A \cdot \exp\left(-\frac{E_a}{RT(t)}\right) \cdot C(t)^n \tag{3}$$

where $A_s(t)$ is the total reaction interface area at time t, m²; $v(t)$ is the reaction rate per unit area, mol/ (m²·s); $V(t)$ is the system volume at time t, m³ ; and $\frac{A_s(t) \cdot v(t)}{V(t)}$ is the total reaction rate per unit volume, mol/ (m³·s).

Thus, a linearized expression for inverting schlieren images of liquid oxygen charges is derived:

$$\ln\left(\frac{A_s(t) \cdot v(t)}{V(t)}\right) = \ln(\alpha A) + n \ln C(t) - \frac{E_a}{RT(t)} \tag{4}$$

By analyzing the local geometric curvature of the flame front, the phase change propagation speed is calculated. Assuming the flame front curve in a two-dimensional image is represented in parametric form $r(\theta, t)$, its local curvature $\kappa(\theta, t)$ is given by:

$$\kappa\left(\theta,t\right)=\frac{|r^2+2(r')^2-r\cdot r''|}{(r^2+(r')^2)^{3/2}} \tag{5}$$

where $\kappa(\theta, t)$ is the curvature in polar coordinates; $r(\theta)$ is the radius at a point on the curve in polar coordinates, m; $r'=\frac{\partial r}{\partial\theta}$ is the first derivative of r with respect to θ, representing the rate of change with angle; and $r''=\frac{\partial^2 r}{\partial\theta^2}$ is the second derivative, representing the rate of change of the rate.

The local propagation speed of the flame front is estimated using a curvature correction model:

$$v(\theta,t)=v_0-D\cdot\kappa(\theta,t) \tag{6}$$

where $v(\theta, t)$ is the normal propagation speed at angle θ and time t, m/s; v_0 is the average propagation speed without curvature, m/s; and D is the interface diffusion coefficient, m^2/s.

In images of the liquid oxygen charge phase change process, the flame region appears as a high grayscale gradient area due to intense density disturbances, while the shock wave front is typically associated with grayscale transition boundaries. To accurately extract these boundary structures, the Canny edge detection algorithm was employed, combined with image gradient enhancement methods for edge identification. The grayscale gradients in the horizontal and vertical directions are expressed as:

$$G_x=\frac{\partial I(x,y)}{\partial x} \tag{7}$$

$$G_y=\frac{\partial I(x,y)}{\partial y} \tag{8}$$

where G_x is the image gradient in the x-direction; $I(x, y)$ is the pixel grayscale value at coordinates (x, y).

The gradient magnitude and direction at edge points are derived as:

$$\theta\left(x,y\right)=\arctan\left(\frac{G_y}{G_x}\right) \tag{9}$$

where $\theta(x, y)$ is the gradient direction angle at point (x, y), rad.

3. Analysis of liquid oxygen phase change results with different absorbent media

The initial combustion stage of liquid oxygen charges with different absorbent media is shown in Fig. 3. Liquid oxygen, as a reactive oxidant, enhances combustion in the absorbent media. Bright regions in the images represent high-temperature combustion zones, with their expansion speed reflecting the combustion rate and flame propagation characteristics of the absorbent media. The left side of the images shows the tissue paper absorbent media, and the right side shows the cotton absorbent media. At 0 μs, electric ignition is initiated. At 610 μs, the tissue paper liquid oxygen charge begins to show a bright combustion zone at the center, indicating the onset of combustion reactions under liquid oxygen's enhancement, concentrated around the ignition head. In contrast, the cotton liquid oxygen charge exhibits a lower initial combustion rate. At 710 μs, the tissue paper charge shows a rapid increase in the area of the bright combustion zone due to increased combustion reaction rates, while the cotton charge, with its denser fiber structure, shows a slower combustion speed and only a slight increase in the combustion zone area. By 810 μs, the tissue paper medium, with its porous layered fiber structure, exhibits a faster liquid oxygen adsorption rate, higher permeability, and greater liquid oxygen adsorption compared to cotton's dense entangled structure under identical oxygen filling times. The tissue paper charge's combustion bright zone rapidly expands to two-thirds of the charge area, while the cotton charge's bright zone shows no significant change due to its lower porosity, forming a heat transfer network that allows rapid heat conduction through internal fibers. Cotton's low porosity creates thermal resistance zones, restricting combustion heat within fiber bundles, resulting in a slower combustion rate compared to tissue paper. From 810 μs to 5,270 μs, during the mid-to-late combustion stage, the combustion zone continues to expand, with both media showing complex brightness distributions, including localized high-brightness and grayscale diffusion areas. The combustion zone edges exhibit irregular expansion, reflecting the instability of the flow field structure during combustion. The tissue paper medium's combustion rate is significantly faster, with the high-brightness combustion zone expanding uniformly from the center to both ends, driven by its porous short-fiber structure, high porosity, and uniform liquid oxygen distribution, which accelerates combustion under liquid oxygen's enhancement, rapidly conducting heat to unreacted liquid oxygen.

The gasification expansion stage of liquid oxygen charges with different absorbent media is shown in Fig. 4. As combustion reactions intensify, the absorbent media release significant heat under liquid oxygen's enhancement, rapidly conducting heat through the fiber framework to unreacted liquid oxygen, rapidly providing sufficient energy for

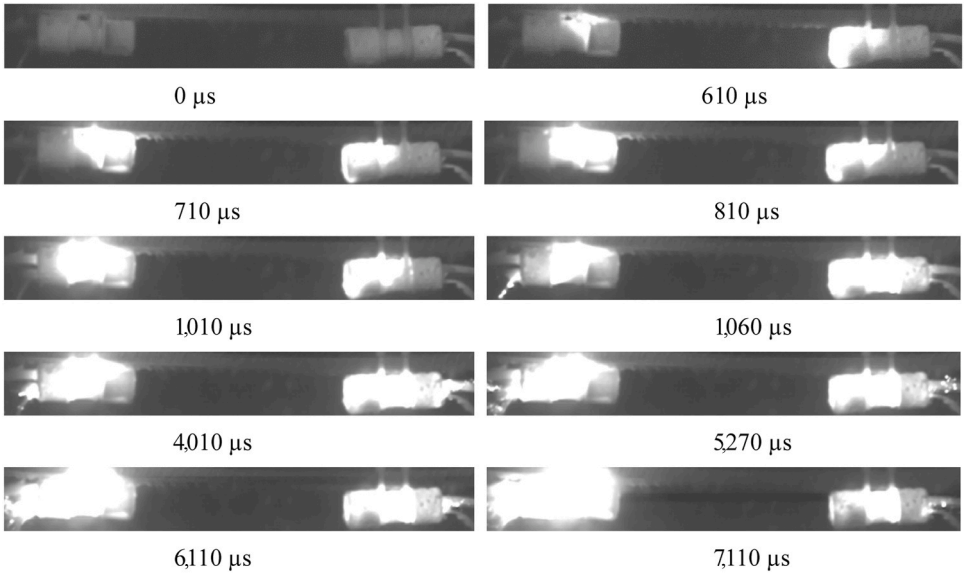

Fig. 3. Initial combustion phase of liquid oxygen charges with different energy-absorbing media.

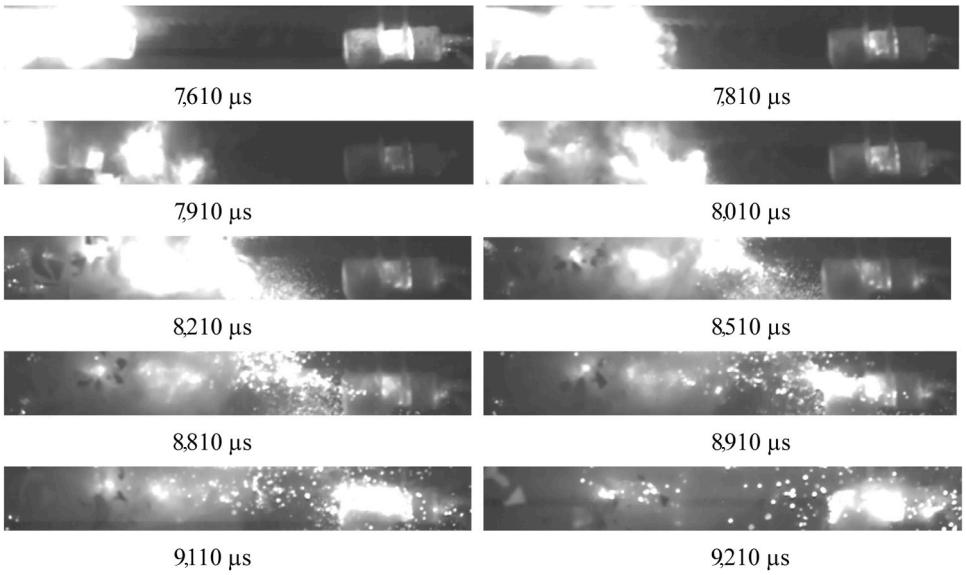

Fig. 4. Gasification-induced expansion stage of liquid oxygen charges with different energy-absorbing media.

gasification. From 7,610 μs to 7,910 μs, the tissue paper liquid oxygen charge, benefiting from its high porosity and interconnected heat transfer network, enters a rapid gasification reaction phase driven by the heat from tissue paper's combustion. Uniform liquid oxygen adsorption results in significant gas release during intense gasification, with high-pressure gases rapidly diffusing, peaking in pressure release, and breaking the storage tube while spreading into the air flow field. In contrast, the cotton liquid oxygen charge, with lower porosity, exhibits slower liquid oxygen penetration, causing a significant phase difference between combustion and gasification. While the tissue paper charge enters rapid gasification expansion, the cotton charge remains in the combustion phase, transitioning from surface to internal fiber combustion. From 8,010 μs to 8,510 μs, the gasification expansion of the tissue paper charge continues, with gas flow diffusing to both sides, releasing significant energy and producing some star-shaped jet flows. Due to insufficient initial combustion heat in cotton, the tissue paper charge's jet sparks provide additional heat to unreacted cotton portions, accelerating cotton's combustion and initiating its gasification expansion. From 8,810 μs to 9,210 μs, the tissue paper charge enters the late gasification expansion stage, with gas release gradually attenuating. Meanwhile, the cotton charge, driven by heat from oxidation reactions, provides substantial energy for unreacted liquid oxygen's phase change, reducing pressure in the storage tube, expanding gas volume, and releasing significant energy, forming a coupled effect of oxidation, heat, phase change, and impact. This indicates that liquid oxygen charges, under the heat release from absorbent media combustion, overcome molecular forces for phase changes, producing oxygen to enhance combustion, while gaseous products expand, generating pressure waves, accelerating combustion through heat conduction and gas expansion, and releasing substantial heat into the air flow field.

The turbulent dissipation stage of liquid oxygen charges with different absorbent media is shown in Fig. 5. From 9,510 μs to 15,710 μs, due to tissue paper's short-fiber structure, the tissue paper charge experiences a broad blasting range under phase change expansion forces, retaining some bright spots post-expansion. Meanwhile, the cotton charge, with uneven adsorption forming localized unsaturated zones, exhibits insufficient combustion. Enhanced by sparks from the tissue paper charge, the cotton charge's combustion rate increases, releasing

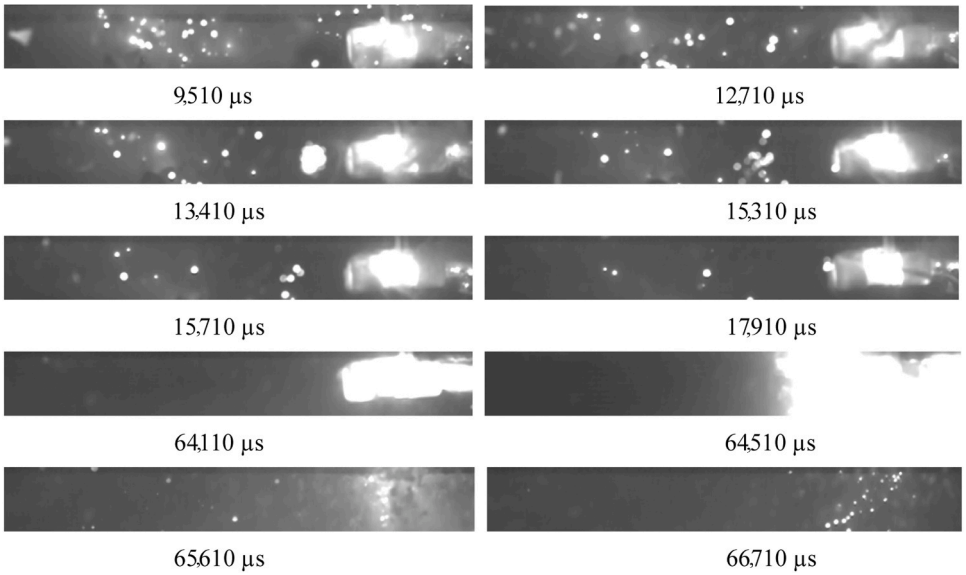

Fig. 5. Turbulent dissipation stage of liquid oxygen charges with different energy-absorbing media.

significant energy and initiating gasification expansion, with gas flow expanding laterally. From 17,910 μs to 66,710 μs, the tissue paper charge's phase change concludes, with the medium almost completely fragmented, showing no significant residue, and turbulent flow gradually dissipating. The cotton charge accumulates energy, sustaining gasification expansion and instantaneous blasting, releasing substantial energy. As pressure releases, the energy attenuates, entering turbulent dissipation, with some cotton fiber fragments remaining due to its dense, long-fiber structure. Thus, cotton's low porosity leads to less and uneven liquid oxygen adsorption, resulting in insufficient combustion. Sparks from the tissue paper charge enhance cotton's combustion, accelerating its gasification expansion. However, cotton's shorter gasification expansion time results in uneven energy release, making energy control challenging and rock-breaking less effective than tissue paper charges.

4. Reaction mechanisms of liquid oxygen charges with different absorbent media

4.1. Shock wave-flame front coupling propagation mechanism

The velocity contour map during the initial combustion stage of liquid oxygen charges with different absorbent media is shown in Fig. 6. Red and yellow regions indicate high-velocity flow fields. From 0 μs to 710 μs, the tissue paper charge exhibits dispersed high-frequency velocity fields, indicating full contact between liquid oxygen and fine short fibers, leading to rapid combustion and energy diffusion, with significant turbulent mixing in the flow field. In contrast, the cotton charge's velocity field is concentrated in localized areas due to uneven liquid oxygen adsorption caused by long fibers. From 810 μs to 1,060 μs, the tissue paper charge's flame front propagation speed is significantly faster than that of the cotton charge, as tissue paper's loose fibers accelerate liquid oxygen diffusion and penetration, while cotton's dense fibers slow liquid oxygen flow, reducing flame diffusion speed. From 4,010 μs to 7,110 μs, the tissue paper charge's high-velocity zone gradually attenuates, indicating a decline in combustion rate, while the cotton charge remains in a low-intensity high-velocity zone, with edges showing low-speed areas. This is due to tissue paper's loose fiber structure accelerating adsorption and diffusion, with faster gasification front propagation compared to cotton, whose dense fibers delay pressure release and slow gasification rates, making tissue paper's combustion rate significantly faster.

The velocity contour map during the gasification expansion stage of liquid oxygen charges with different absorbent media is shown in Fig. 7. As the absorbent media in the liquid oxygen charges combust and release significant heat, unreacted liquid oxygen undergoes gasification expansion in a high-temperature environment. From 7,610 μs to 8,210 μs, the tissue paper liquid oxygen charge undergoes gasification expansion, during which the fine fibers of tissue paper are easily fragmented by the phase change impact, leading to rapid energy dispersion. The coupling of fine fibers and liquid oxygen phase change accelerates the fragmentation process, with high-velocity zones becoming sparse as the gasification expansion energy is released, resulting in some attenuation of the velocity field. During the same period, the cotton liquid oxygen charge, due to the energy-binding effect of its coarse cellulose fibers, adsorbs less liquid oxygen compared to the tissue paper medium, prolonging the combustion process. The insufficient heat from the limited liquid oxygen adsorption is inadequate to trigger gasification expansion in the cotton charge. From 8,510 μs to 9,210 μs, the high-velocity zone of the tissue paper liquid oxygen charge gradually diffuses to the edges, showing a uniform distribution of blue low-speed zones, indicating that the tissue paper charge enters a stable low-speed gasification expansion stage with thorough reactions between the tissue paper fibers and internal liquid oxygen. During the same period, sparks from the gasification jets of the tissue paper charge splash onto the cotton liquid oxygen charge, accelerating its combustion rate. Consequently, the development speed of the high-velocity zones in the cotton liquid oxygen charge is slower than that of the tissue paper charge, with a noticeable lag.

The velocity contour map during the turbulent dissipation stage of liquid oxygen charges with different absorbent media is shown in Fig. 8. From 9,510 μs to 17,910 μs, the tissue paper liquid oxygen charge on the left continues to develop through the gasification expansion process,

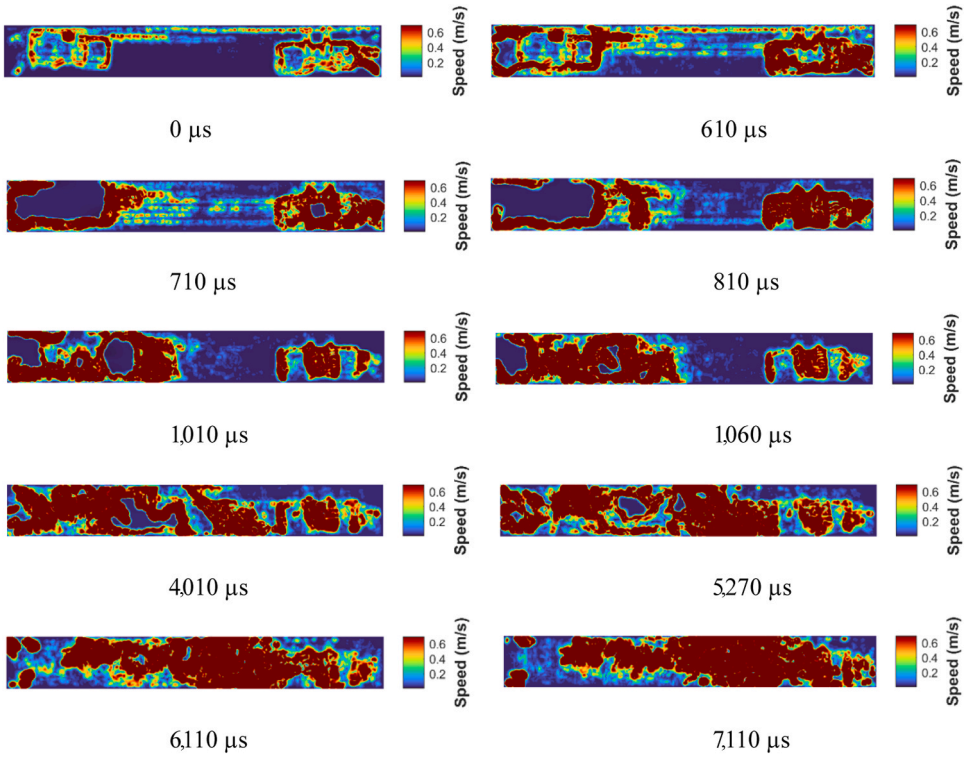

Fig. 6. Velocity contour map during initial combustion phase of liquid oxygen charges with different energy-absorbing media.

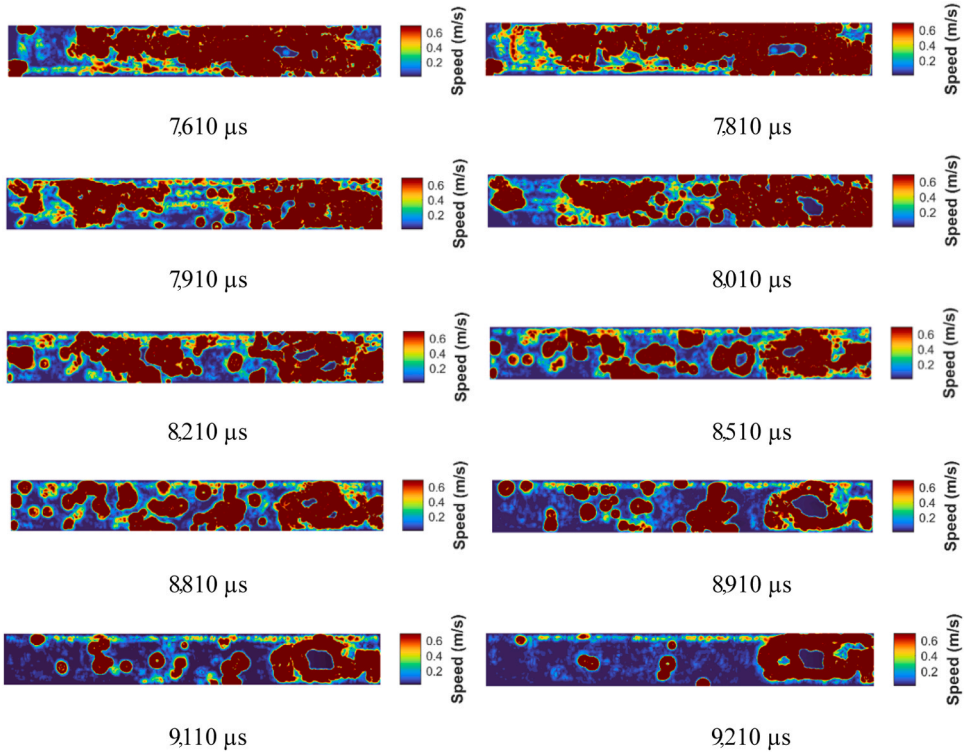

Fig. 7. Velocity contour map during gasification-induced expansion stage of liquid oxygen charges with different energy-absorbing media.

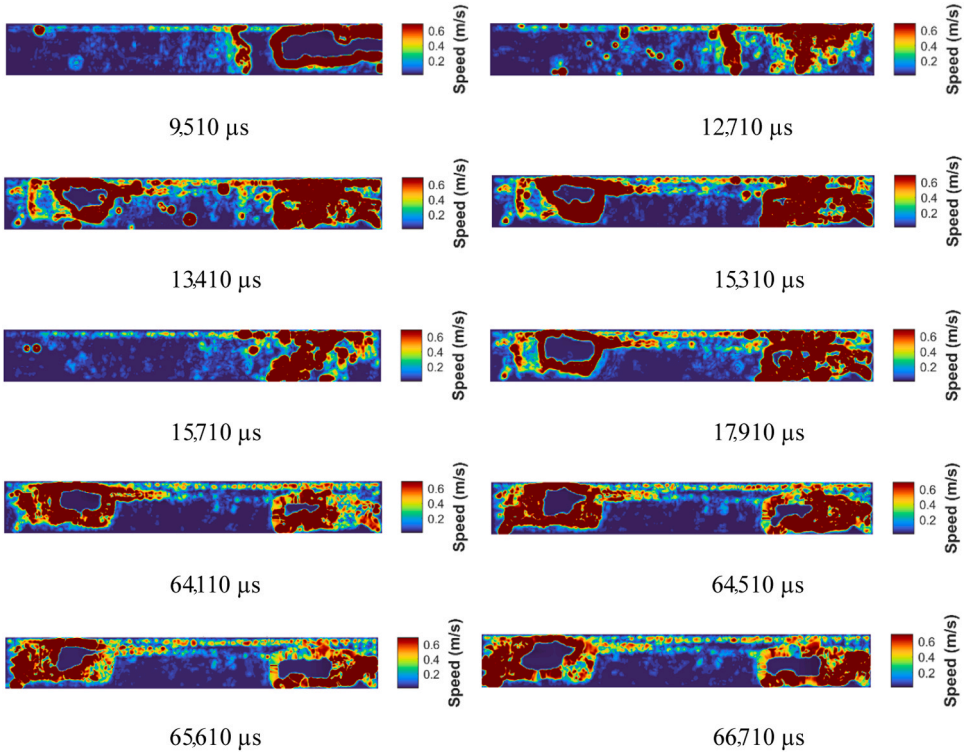

Fig. 8. Velocity contour map during turbulent dissipation stage of liquid oxygen charges with different energy-absorbing media.

with energy release gradually dissipating and velocity decreasing. During the same period, the cotton liquid oxygen charge on the right experiences an accelerating combustion reaction rate, with the area of high-velocity zones gradually increasing. From 64,110 μs to 66,710 μs, the turbulent fluctuations of the tissue paper charge weaken, approaching a steady state. In contrast, the cotton charge, having been in the combustion phase, accumulates sufficient heat to trigger an instantaneous gasification expansion reaction in the unreacted liquid oxygen. During this process, the high-velocity zones of the cotton charge continue to develop until the energy dissipates. Compared to the tissue

paper charge, the cotton charge exhibits a smoother energy absorption process with slower turbulent motion, while the tissue paper charge shows rapid increase and decay in turbulent motion, highlighting significant differences in the regulation of thermodynamic coupling and energy release patterns during liquid oxygen gasification between the two absorbent media.

4.2. Thermodynamic coupling characteristics and energy release patterns

The temperature contour map during the initial combustion stage of liquid oxygen charges with different absorbent media is shown in Fig. 9. Red and orange regions indicate lower relative temperatures, while yellow and white regions indicate higher temperatures. From 0 μs to 1,010 μs, the tissue paper liquid oxygen charge on the left exhibits a uniform temperature distribution. As time progresses, the high liquid oxygen content in the tissue paper's fiber structure enhances combustion, leading to rapid expansion of high-temperature light-colored zones and accelerated temperature field changes, indicating rapid combustion and heat release. In contrast, the cotton liquid oxygen charge on the right shows high-temperature light-colored zones localized to specific areas, reflecting lower liquid oxygen adsorption and slower heat transfer due to its dense porous structure, resulting in less intense initial combustion. From 1,060 μs to 7,110 μs, the high-temperature zone of the tissue paper charge expands across the entire charge and surrounding areas, then gradually decreases, indicating heat dissipation. The cotton charge shows slight diffusion of high-temperature zones, reflecting slower heat absorption due to its long-fiber structure. Comparing the initial combustion processes of the two absorbent media, the temperature peaks of the tissue paper charge are more concentrated at the charge center, indicating a more intense phase change reaction compared to the cotton charge. Due to tissue paper's high porosity and loose short-fiber structure, its liquid oxygen adsorption rate is faster than that of cotton, with a significantly higher energy release rate. Consequently, the combustion phase of the tissue paper charge is shorter, while the cotton charge's combustion rate is much slower due to insufficient liquid oxygen adsorption.

The temperature contour map during the gasification and expansion stage of liquid oxygen charges with different absorbent media is shown in Fig. 10. As can be seen from the figure, in the time period of 7,610 μs to 8,510 μs, the high-temperature bright zones of the tissue paper liquid oxygen charge on the left are concentrated. With the passage of time, the central high-temperature zone gradually diffuses and the temperature at the edge rises, which indicates that during the gasification and expansion process, heat is conducted from the charge zone to the surrounding areas. Meanwhile, the short-fiber structure of tissue paper accelerates energy release, and the uniformity of the temperature field increases. During the same period, the distribution of the high-temperature zone of the cotton liquid oxygen charge on the right gradually expands, and the combustion reaction continues. Its dense porous structure enables the slow release of internal heat. In the time period of 8,810 μs to 9,210 μs, for the bright zones of the tissue paper liquid oxygen charge on the left, due to the rapid energy release during the gasification and expansion process, the temperature is concentrated in the early stage of expansion, and then the temperature field zone becomes uniform. During the same period, for the cotton liquid oxygen charge on the right, its internal dense structure results in a slow internal combustion heat release rate; as the combustion reaction proceeds, the area of the high-temperature zone continues to expand.

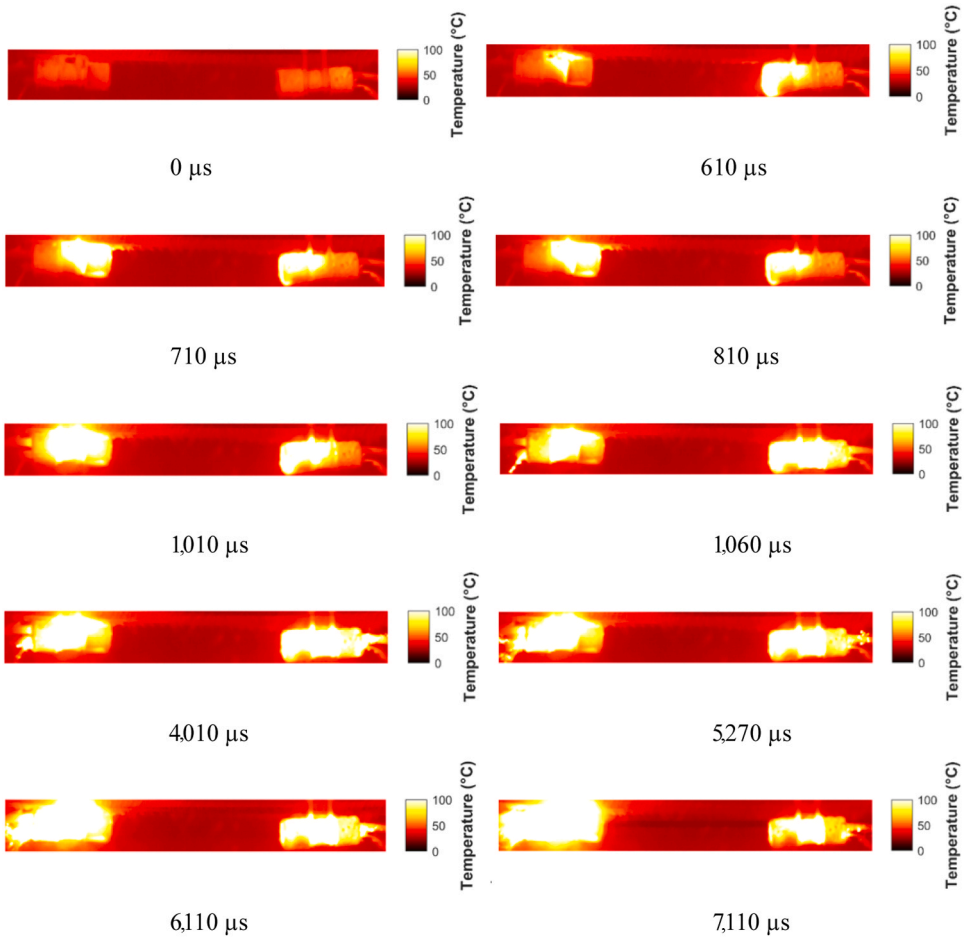

Fig. 9. Temperature contour map during initial combustion stage of liquid oxygen charges with different energy-absorbing media.

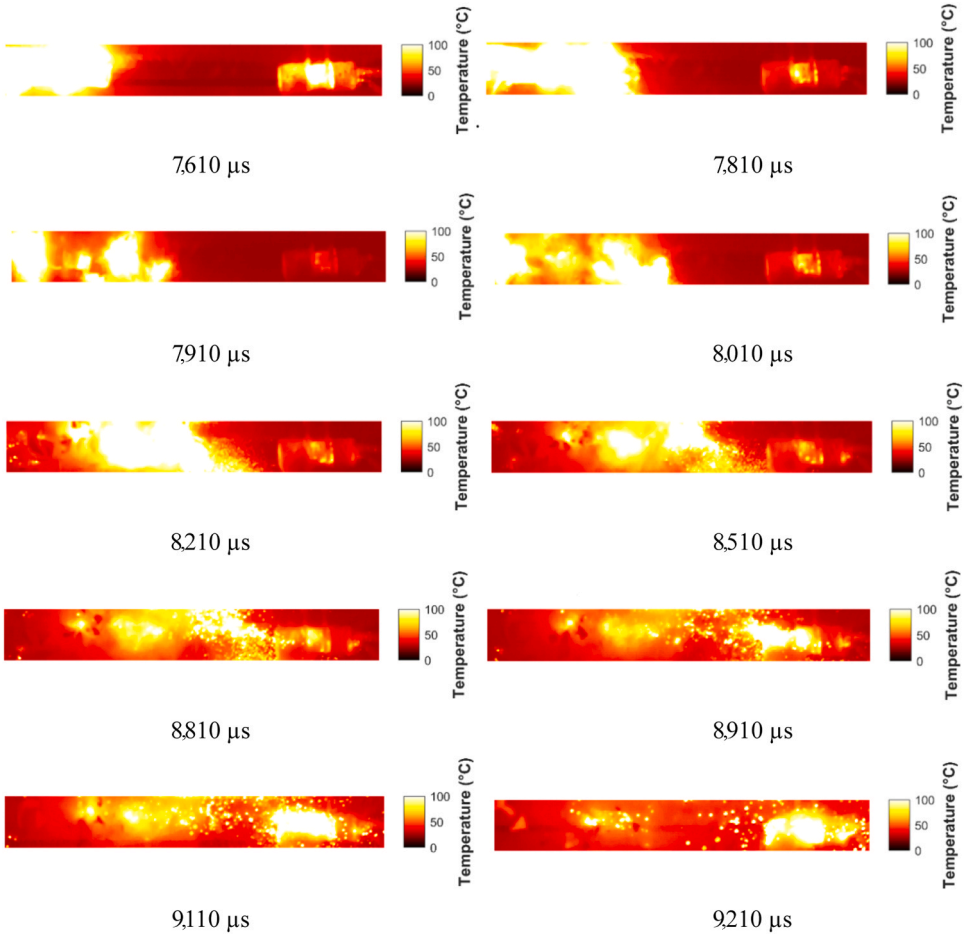

Fig. 10. Temperature contour map during vaporization-expansion stage of liquid oxygen charges with different energy-absorbing media.

The temperature contour map during the turbulent dissipation stage of liquid oxygen charges with different absorbent media is shown in Fig. 11. From 9,510 μs to 17,910 μs, the high-brightness temperature field zones of the tissue paper liquid oxygen charge on the left gradually diffuse, indicating the end of the gasification expansion phase and the entry into the turbulent dissipation process. During the same period, the high-brightness temperature field zones of the cotton liquid oxygen charge on the right continue to expand. As the cotton charge sustains continuous combustion, it accumulates sufficient heat, triggering a gasification expansion reaction in the unreacted liquid oxygen, releasing significant energy. The high-temperature zones rapidly diffuse and gradually attenuate. Consequently, the tissue paper charge, due to its short-fiber structure, allows rapid heat conduction through the fiber framework from the combustion of liquid oxygen and the absorbent media, leading to concentrated high temperatures initially and rapid cooling later. In contrast, the cotton charge, with its lower porosity, experiences alternating heat transfer within its structure, prolonging the combustion duration and causing an instantaneous temperature rise in the temperature field during the gasification expansion phase.

5. Conclusions

Based on transient phase change reaction images and grayscale temporal feature analysis obtained through high-speed photography, this study conducted experimental research on the reaction processes of liquid oxygen charges with different fiber-structured absorbent media, yielding the following conclusions:

(1) The microscopic fiber structure of the absorbent media determines the transient phase change reaction process of liquid oxygen charges, which is divided into three stages: initial combustion, gasification expansion, and turbulent dissipation. Tissue paper, with its loose, porous structure and high permeability, promotes uniform liquid oxygen adsorption and diffusion, resulting in steady energy release and a relatively continuous reaction process. In contrast, cotton's dense fiber network significantly reduces permeability, hindering uniform liquid oxygen infiltration and gas product release, leading to concentrated energy accumulation in localized areas and intense but delayed energy release.

(2) Relative velocity and temperature fields derived from grayscale image inversion clearly show that tissue paper's short-fiber structure, with its large specific surface area and interconnected pores, ensures uniform liquid oxygen adsorption and distribution, resulting in high synchronization and spatially uniform energy release across the charge. In contrast, cotton's dense long-fiber structure causes significant uneven liquid oxygen adsorption, leading to localized intense compression and enhanced turbulent dissipation.

(3) The effectiveness of different absorbent media in rock breaking stems from their energy release characteristics. Tissue paper-based liquid oxygen charges exhibit steady, uniform, and highly synchronized energy release. Although cotton can generate higher local peak pressures, its delayed, concentrated, and severely uneven energy release prevents effective energy

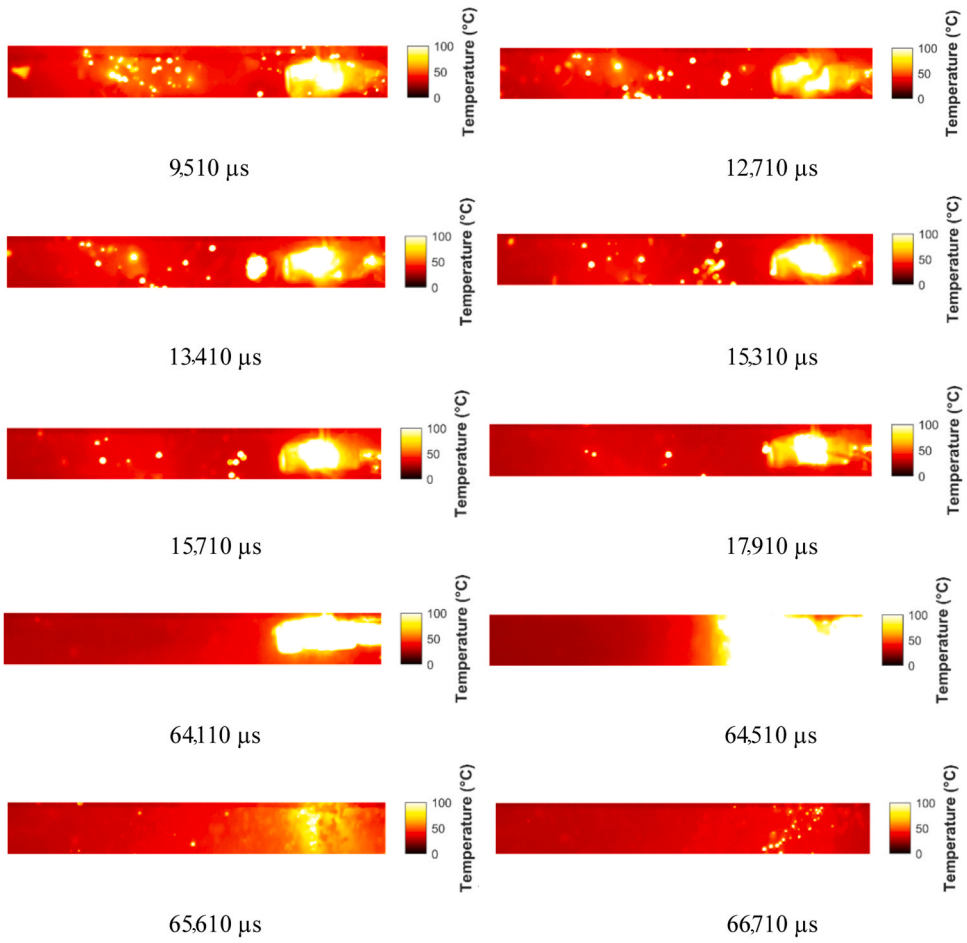

Fig. 11. Temperature contour map during turbulent dissipation stage of liquid oxygen charges with different energy-absorbing media.

coupling, with most energy consumed in non-uniform structural responses and ineffective turbulence, resulting in significantly lower energy utilization efficiency compared to tissue paper.

CRediT authorship contribution statement

Yanbing Wang: Writing – original draft. **Xue Li:** Writing – original draft. **Dairui Fu:** Conceptualization. **Kangcheng Li:** Methodology. **Dongchen Wang:** Methodology. **Haitao Le:** Writing – review & editing. **Linsheng Zhao:** Supervision. **Chuanhao Lv:** Resources. **Yuanyuan Liu:** Resources. **Bo Xu:** Validation. **Zungang Liu:** Visualization. **Xiao Wang:** Validation.

Declaration of Competing Interest

The authors declare that they have no known competing financial interests or personal relationships that could have appeared to influence the work reported in this paper.

Acknowledgements

The study was supported by the National Natural Science Foundation of China (No. 52574184), Fundamental Research Funds for the Central Universities (No. 2025JCCXLJ01).

Data availability statement

All data included in this study are available upon reasonable request by contact with the corresponding author.

References

[1] J.J. Ji, H.T. Li, F.M. Wu, et al., Fractal characteristics of rock fragmentation under impact load, J. Vib. Shock 39 (13) (2020) 176–183 (in Chinese).
[2] Y. Yang, R.S. Yang, J. Chen, et al., Advancements and future prospects in the fundamental theories of rock blasting research I —Constitutive relationships, Chin. J. Eng. 46 (11) (2024) 1931–1947 (in Chinese).
[3] J.P. Wei, Y.B. Cai, Y. Liu, et al., Progress and trends in non-tool rock breaking theory and technology, J. China Coal Soc. 49 (2) (2024) 801–832 (in Chinese).
[4] L.J. Chen, J.M. Feng, X.C. Wu, Experimental research on transient rock breaking characteristics of high-energy gas, Chin. J. Rock Mech. Eng. 39 (S2) (2020) 3271–3277 (in Chinese).
[5] X.L. Zhao, B.X. Huang, J. Xu, Experimental investigation on the characteristics of fractures initiation and propagation for gas fracturing by using air as fracturing fluid under true triaxial stresses, Fuel 236 (2019) 1496–1504.
[6] H.B. Chu, M.F. Yu, S.Y. Yan, et al., Comparison analysis on high-pressure gas crackingand explosive blasting vibration, Blasting 39 (4) (2022) 177–185 (in Chinese).
[7] Y.L. Lu, M.Q. He, B.Z. Wu, et al., Experimental and theoretical analysis of hydraulic fracturing and gas fracturing of rock under true triaxial compressions, Eng. Fract. Mech. 234 (2020) 107100.
[8] L. Qin, P. Wang, S.G. Li, et al., Reconstruction and degradation mechanism of three-dimensional CT cracks in coal under the cycle impact of liquid CO_2 high-temperature steam, J. China Coal Soc. 49 (S1) (2024) 304–313 (in Chinese).

[9] H.T. Wang, J.H. Yang, J.L. Tan, et al., Research on multi-field coupling evolution law of liquid CO_2 filling in difficult water injection seams, Coal Sci. Technol. 52 (S2) (2024) 121–130 (in Chinese).
[10] X.S. Cheng, H.D. Liu, S.L. Zhang, et al., Test on filling mass of liquid CO_2 phase transition blasting in rock cutting, China Civ. Eng. J. 56 (7) (2023) 137–146 (in Chinese).
[11] H.F. Lin, B.T. Li, S.G. Li, et al., Development and application of true triaxial experimental system for the whole process of coal fracturing induced by liquid nitrogen injection, Chin. J. Rock Mech. Eng. 44 (2) (2025) 276–291 (in Chinese).
[12] H.F. Lin, B.T. Li, S.G. Li, et al., A thermal-hydraulic-mechanical-damage coupling model of layer coal fracturing by liquid nitrogen, Chin. J. Rock Mech. Eng. 43 (5) (2024) 1110–1123 (in Chinese).
[13] J.R. Wang, Y.J. Zhao, Y.C. Li, et al., Analysis of mechanical properties, permeability and fracturing mechanism of coal samples at different fracturing time of liquid nitrogen, Coal Sci. Technol. 51 (6) (2023) 101–110 (in Chinese).
[14] Z. Lei, Y.B. Wang, D.R. Fu, et al., Research on rock fracturing technology based on liquid oxygen energy storage, Blasting 42 (1) (2025) 151–158 (in Chinese).
[15] Y.B. Wang, X. Li, C.Y. Que, et al., Study on the flow field structure and pulsation characteristics of liquid oxygen transient expansion directional energy release gas, J. China Univ. Min. Technol. 54 (3) (2025) 609–622 (in Chinese).
[16] H.H. Zeng, Y.L. Xie, Y. Hu, et al., Calculation method of wall pressure for uncoupled liquid oxygen explosion for rock fracturing, Blasting 42 (2) (2025) 146–157 (in Chinese).
[17] S.S. Wang, Research on safety issues and control measures of gas blasting technology in China, Eng. Blasting 31 (2) (2025) 47–53 (in Chinese).

Yanbing Wang is an Associate Professor and a YUEQI Young Scholar at China University of Mining and Technology (Beijing). He was selected for the China Association for Science and Technology's Young Talent Support Project. He is mainly engaged in teaching and research work in underground engineering construction and rock dynamics. As the person in charge, he has presided over five projects of the National Natural Science Foundation of China (NSFC) Youth Fund, the China Postdoctoral Science Foundation (CPFSF) Special Grant, the China Postdoctoral Science Foundation (CPFSF) Upper Level Project (First Class), etc., and participated in six projects of the National Key Research and Development Programme (NKRDP) and the National Natural Science Foundation of China (NNSF) as the main researcher, and published more than 40 academic papers.